Phase morphology and interfacial characteristics of polycarbonate/acrylonitrile-ethylene-propylene-diene-styrene blends compatibilized by styrene-maleic anhydride copolymers

Shengming Li, Rong Tang, Bo Jing, Wenli Dai, Xiaoxuan Zou

Institute of Polymer Science and Engineering, College of Chemistry, Xiangtan University, Xiangtan 411105, Hunan Province, China
Correspondence to: X. Zou (E-mail: zouxiaoxuanxtu@163.com)

ABSTRACT: Blends of polycarbonate (PC) and acrylonitrile-ethylene-propylene-diene-styrene (AES) were reactive compatibilized by styrene-maleic anhydride copolymers (SMA). The changes in phase morphology and interfacial characteristics of the blends as a function of maleic anhydride content of SMA and the concentration of compatibilizer have been systematic studied. The occurrence of reaction between the terminal hydroxyl groups of PC and the maleic anhydride (MA) of compatibilizer was confirmed by fourier transform infrared (FTIR) spectroscopy. A glass transition temperature (T_g) with an intermediate value between $T_{g(AES)}$ and $T_{g(PC)}$ was found on differential scanning calorimeter (DSC) curves of PC/AES blends compatibilized with SMA contains high levels of MA. Furthermore, at lower compatibilizer content, increase of the compatibilizer level in blends result in decreasing gap between two T_{gs} corresponding to the constituent polymers. Small angle X-ray scattering (SAXS) test results indicated that compatibilizer concentration for the minimum of blend interface layer's thickness was exactly the same as it was when compatibilized PC/AES blend exhibited optimal compatibility in DSC test. The observed morphological changes were consistent well with the DSC and SAXS test results. A new mechanism of interfacial structural development was proposed to explain unusual phenomena of SMA compatibilized PC/AES blends. © 2015 Wiley Periodicals, Inc. J. Appl. Polym. Sci. 2015, 132, 42103.

INTRODUCTION

Polycarbonate (PC) is widely used as a high-performance thermoplastic with good mechanical properties, transparency, and high heat resistance properties. However, its high melt viscosity, notch sensitivity, and residual stress resulting from process restrict its application. Efforts have been made to overcome the limitations of PC through the method of blend PC with thermoplastics, of which ABS is most common.[1–5] Because of complementary properties of the components, PC/ABS blends have received considerable attention in engineering applications.[6–12] However, PC/ABS blends are not suitable for outdoor use due to butadiene rubber contains a double bond in ABS repeat unit. When PC/ABS blend exposed to ultraviolet or sunlight radiation, it undergoes thermo-oxidative degradation. As another attractive rubber-toughened thermoplastic, acrylonitrile-ethylene-propylene-diene-styrene (AES) is chemically similar to ABS, except that the polybutadiene rubber is replaced by ethylene-propylene-diene (EPDM) rubber.[13,14] AES has comparative mechanical properties with ABS. Moreover, the presence of saturated EPDM rubber enables AES to exhibit good weather-resistive and thermal stability during processing.[15–18]

Just as ABS presents two-phase structure, AES has a microstructure of EPDM particles dispersed in the matrix of styrene-acrylonitrile (SAN). The approximate calculated solubility parameters of PC, SAN, and EPDM are respectively 9.4–9.6, 9.5–9.6, and 7.5–8.3 $(cal/cm^3)^{.1/2}$ The solubility parameter difference between PC and SAN is small, whereas the difference between EPDM and PC is out of the generally accepted range for polymer mixing.[19] Therefore, from the solution parameter point of view, compatibility of PC and AES is not good. The applications of blends with less compatibility are often limited because of their poor adhesion at the weld. Previous works have demonstrated that PC and ABS is shown to exhibit rapid phase coarsening and lowering material properties at an elevated temperature.[20–22] Since the chemical similarity between ABS and AES, it is considered that PC/AES blends also tend to form coarse and unstable phase morphology at a processing temperature. Drawbacks of the PC/AES blends have motivated the

Table I. Typical Physic and Chemical Properties of SMA Resin

Copolymer	Acid number mg KOH/g	MA content (wt %)	Molecular weight (g/mol)	M_w/M_n	T_g (°C)
SMA1	480	49	$M_n = 2000, M_w = 5500$	2.75	155
SMA2	355	32	$M_n = 3000, M_w = 7500$	2.5	135

search for an appropriate compatibilizer for this system. As aforementioned, the constitution and structure characteristics of ABS and AES are very similar. It is expected that compatibilizers have great effect for the PC/ABS blends would also be adequate for PC/AES blends. There have been many literatures dealing with the efficient reactive compatibilization of PC/ABS blends with copolymers containing maleic anhydride (MA) groups.[23–27]

The compatibilizing method used in these studies is based on the fact that the SAN phase tends to form interface with the polycarbonate (PC) in the PC/AES blends. Taking into consideration this interfacial characteristic, for the compatibilization of these systems, we have used SMA. This compatibilization strategy relies on the assumption that this styrene based compatibilizer are compatibility with AES because of the presence of structurally similar styrene units in the polymer backbone, meanwhile the MA groups of them reacted with terminal hydroxyl groups of PC during the melt processing of the blends. This could lead to the formation of grafted copolymers (PC-g-SMA) at the interface of PC/AES blends, thus improve interface performance between two components and reduce the phase coarsening. To our knowledge, utilizing diblock copolymers incorporate MA as a compatibilizer for PC/AES blends are rarely seen in the literature.

In present study, similar SMA copolymers were used in an attempt to promote the compatibilization of PC/AES blends. Evidence of the formation of interfacial grafted copolymers by in situ reactions was sought. Moreover, the influences of SMA content and composition on the properties of the blends were also analyzed from the perspectives of interfacial characteristics, thermology, morphology, mechanic, and rheology.

EXPERIMENTAL

Materials
PC (Lexan 144R-111 of GE Company, USA) with density of 1.19 g/cm³ and MFI of 10.5 g/10min (at 300°C, 1.2 kg), and AES (HW600HI of Kumho Petrochemical Company, Korea) with density of 1.04 g/cm³ and MFI of 15 g/10 min (at 220°C, 10 kg) are supplied as pellets. The internal AES composition is 36 wt % EPDM and the SAN used as matrix for the AES. SMA (SMA1 and SMA2 of Sartomer Company, USA) are supplied as powder form and their characteristics are listed in Table I. All polymers are commercial products and used without further purification.

Melt Blending and Injection Molding
To prepare the blends, AES and SMA were dried at 90°C, 85°C respectively in a vacuum oven for 8 h, and PC pellets were dried for a minimum of 12 h under vacuum at 100°C before melt processing. The SMA powder were thoroughly mixed and

melt-compounded with PC or 70/30 (wt/wt) PC/AES blends by using a corotating twin-screw reactive extruder (Nanjing rubber machinery factory, SJSH-30, China). In addition, 0.5 wt % thermal stabilizer (Irganox 1010 of Ciba-Geigy Company, Switzerland) was added to the blends during mixture. The PC/SMA blends weight ratios were the following: 95/5, 90/10, 85/15. The SMA modified PC/AES (70/30) blends were coded as XXPhr SMA1 or XXPhr SMA2, where XX stands for the weight portion of the compatibilizer. The screw speed was maintained at 100 rpm for all runs, and the eight controlled temperature zones from the first heating zone to the die were set at 225, 230, 235, 240, 235, 230, 225, and 220°C, respectively. The extrudate was cooled in a water bath keep at room temperature, and subsequently granulated by a strand pelletizer. Pellets were dried in a vacuum oven at 80°C for 12 h prior to injection molding. Test specimens for determining the mechanical properties and annealing experiments were prepared using an injection molding machine (Ningbo Haitian plastics machinery Company, HTB-80, China). The four zone temperatures of the barrel were kept constant at 240, 245, 250, and 245°C, respectively, and the nozzle was set at 235°C.

Isothermal Annealing
Annealing was performed using an accurate temperature controlled hydraulic press with sufficient pressure to promote melting. PC/AES (70/30) blend and 9Phr SMA1 were annealed at 240°C. For the PC/AES (70/30) blend, the annealing times used were 0, 2, 6, 10, and 14 min; the samples are indicated by A0, A2, A6, A10, and A14, respectively. For the 9Phr SMA1, the annealing times used were the same: this is indicated by B0, B2, B6, B10, and B14, respectively. Upon removal from the press, all samples were immediately quenched in liquid nitrogen to "freeze-in" the morphology.

Fourier Transform Infrared Spectroscopy
Fourier transform infrared (Perkin-Elmer, Nicolet-6700, USA) spectrum was recorded between 600 and 4000 cm⁻¹ with 32 scans at a resolution of 2 cm⁻¹. To analyze the reactive interfacial compatibilization, the samples were films drawn from the blends when they were still in the melt state and then extracted with acetone under stirring at ambient temperature for 72 h to remove the free SMA. The collected residues were ground with KBr powder at the 1 : 100 sample/KBr weight ratios and then molded into disks using a press. The disks were oven-dried under vacuum to further remove residual solvent and moisture.

Small Angle X-ray Scattering Studies
Small Angle X-ray Scattering (Rigaku, D/Max-2500v/PC, Japan) measurements were performed to estimate the thickness of the interface layer formed between the PC and AES boundary. A copper target X-ray tube ($\lambda = 1.542$ Å) operated at 40 kV and
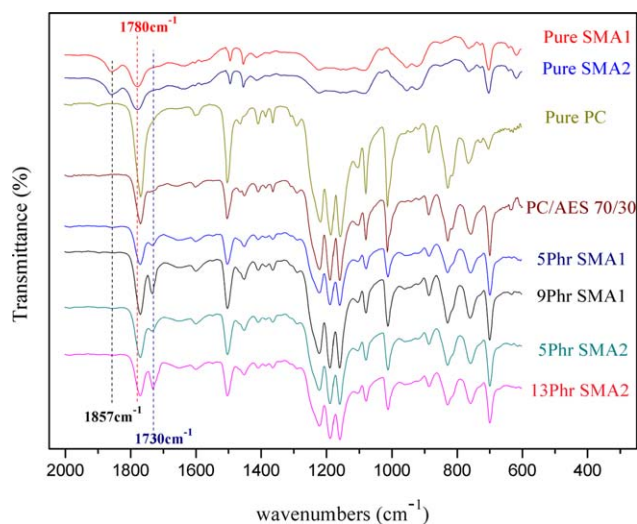
Figure 1. FTIR spectra of SMA, PC, and SMA compatibilized PC/AES (70/30) blends. [Color figure can be viewed in the online issue, which is available at wileyonlinelibrary.com.]

200 mA was used as the source of radiation. The intensity distribution was measured by a low-angle X-ray camera with a step scanning device and a scintillation counter. The intensity scattered by a sample was recorded from $0.3°$ to $2°$ with a step of $0.01°$ and a step time of 1 s. The measured intensity distributions were corrected for air scattering before further analysis.

Morphology Observation

Scanning electron microscopy (JEOL, JSM-6610LV, Japan) was used to observe the morphology of the minor phase embedded in the PC matrix in order to obtain information on phase miscibility, and distribution. The samples were first cryo-fractured in liquid nitrogen. Then acid etching was done to remove minor AES dispersed phase in the PC matrix. An acid aqueous solution of 120 mL of H_2SO_4, 5 g of CrO_3, and 30 mL of H_2O at $85°C$ for 10 min to oxidize the AES phase. These etching treatments were made to obtain the necessary contrast between the phases. Before the observation both types of specimens were coated with an Au/Pd alloy. The acceleration voltage was 30 kV.

Thermal Analysis

DSC (TA Instruments, DSC-Q10, USA) performed under a nitrogen purge was used to investigate the thermodynamic behavior of the SMA modified PC/AES blends. Weight of Specimens was about 10 mg. The temperature of the sample was raised from 30 to $200°C$ at a rate of $20°C$/min, and then by isothermal for 5 min in order to erase its thermal history. Then, the sample was cooled down from 200 to $50°C$ at a rate of $10°C$/min. Finally, the sample was heated up again from 50 to $180°C$ at a rate of $10°C$/min. The positions of their enthalpy relaxation peaks were recorded.

Rheological Analysis

The rheological measurements were performed on an oscillatory rheometer (TA Instruments, ARES-G2, USA) in the parallel plate mode. Experiments were carried out with a 25 mm diameter disk. The sample was loaded between the parallel plates and melted at $250°C$ for 3 min. The parallel plates subsequently compressed the sample to 1 mm thick prior to each test. The

linear viscoelastic range of deformations was characterized by strain sweep test at the frequency of 1 rad/s covering a large strain scope from 0.1 to 100%. The dependence of the melt's complex viscosity on frequency of different samples was evaluated within their respective linear viscoelastic zones. The oscillatory frequency covered was from 0.01 to 100 rad/s.

Mechanical Properties

Tensile tests were measured on a microcomputer controlled Universal Tester (Reger Instruments, RGD-5, China) according to the procedure of ASTM D638 at room temperature with a crosshead rate of 50 mm/min. Flexural properties were also performed on the same RGD-5 universal testing machine at room temperature following the procedure described in ASTM D790. The crosshead speed was 20 mm/min. All the data were taken as averages of at least five measurements.

RESULTS AND DISCUSSION

Fourier Transform Infrared Spectroscopy

The infrared spectrums of SMA, PC, and SMA compatibilized PC/AES blends are compared in Figure 1. Pure SMA exhibited an intensive absorption band near 1780 cm^{-1} and a weak band near 1857 cm^{-1}. These two absorbance peaks were ascribed to symmetric stretching and asymmetric stretching vibrations of anhydride carbonyl (C=O).[28,29] In comparison, spectrums of SMA compatibilized PC/AES (70/30) blends were different from that for pure SMA, pure PC, and PC/AES (70/30) blend. The biggest difference is that anhydride carbonyl peaks at 1780 and 1857 cm^{-1} were hardly noted while an absorption peak at 1730 cm^{-1} corresponds to the stretching vibrations of ester C=O in newly formed PC-g-MA-co-St chains present in the SMA compatibilized PC/AES (70/30) blends. Moreover, with the increase of SMA concentration, the relative intensity at 1730 cm^{-1} was enhanced, indicating an increase of PC-g-MA-co-St concentration in blends. The above results showed obvious evidences that the hydroxyl terminated of PC reacted with the carboxyl groups (Figure 2), which were generated by ring opening of cyclic anhydrides groups.

Determination of the Interface Thickness by SAXS

Macroscopic properties of incompatible and partially compatible systems are closely depending on domain size and interfacial
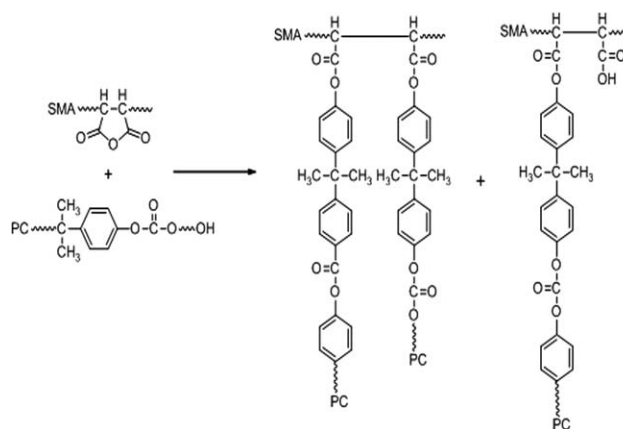
Figure 2. The formula of reaction between maleic anhydride groups of SMA and hydroxyl terminated of PC.
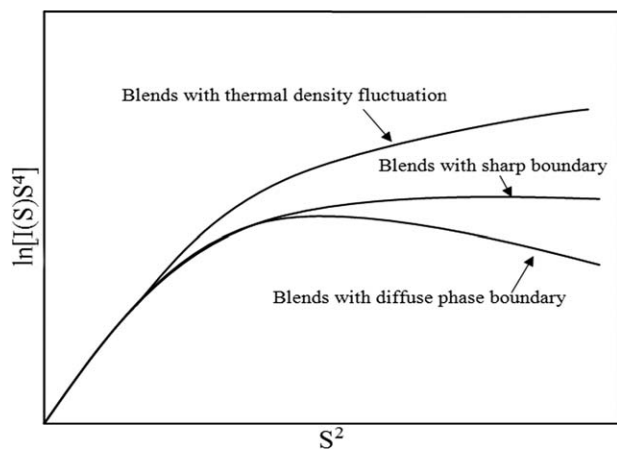
Figure 3. Schematic diagrams of Porod's law and deviations from Porod's law.

Figure 4. Porod plot in the form of $\ln[I(S)S^4]$ as function of S^2 for SMA1 compatibilized PC/AES (70/30) blends. [Color figure can be viewed in the online issue, which is available at wileyonlinelibrary.com.]

thickness. In this section, the changing trend of interfacial thickness will be discussed and analyzed. The method used in this article to determine the interfacial thickness was presented in detail by Koberstein et al.[30] The limiting behavior of ideal two-phase system's scatter intensity at large value of S ($S = 4\pi\sin\theta/\lambda$), is described by the Porod relation:[31]

$$\lim_{S\to\infty}[I(S)] = \frac{K}{S^4} \qquad (1)$$

where S is the scattering vector and $I(S)$ is the scattering intensity at S. K is the so-called Porod-law constant. In other words, eq. (1) suggest that for ideal two-phase systems with sharp boundaries, when S sets to a high value, the product of $I(S)S^4$ reaches a constant value (Figure 3).

However, in real polymer systems, the product $I(S)S^4$ of does not reach a constant. The existence of thermal density fluctuation results in an improvement of scattering at high angles bringing about plot of $I(S)S^4$–S^2 to have a positive slope. On the other hand, the diffuse phase boundary is responsible for negative deviation from Porod's law. Therefore, a modified Porod equation is derived.[30]

$$\lim_{S\to\infty} S^4 I(S) = K\exp(-4\pi\delta_b^2 S^2) \qquad (2)$$

In this article, E will be used as a measurement of the interfacial layer thickness.

$$E = (12\delta_b)^{1/2} \qquad (3)$$

Figures 4 and 5 show a correlation between $\ln[I(S)S^4]$ vs. S^2 for the SMA compatibilized PC/AES blends, and a linear fitting at high-s region are given, this linear fit was used for estimation of the interfacial thickness of this sample. The calculated thickness of interfacial zone is reported in Table II. The data revealed that there was significant change in the value of interfacial thickness with the variation of SMA content in PC/AES blends. This indicates the content of compatibilizer added into blends affect significantly the interfacial characteristics of this blending system.

As can be seen from Table II, with the increase content of compatibilizer in blends, the value of interfacial thickness is found to: first increase, then decrease to a specific value and increase
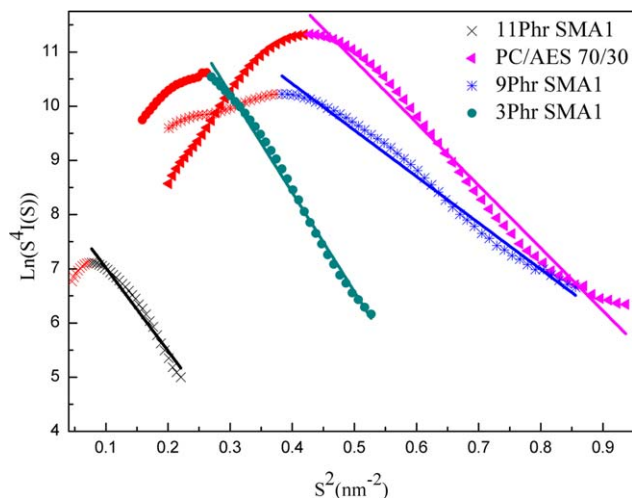
again (Figure 6). In addition, the minimum thickness of interface layer were essentially unchanged (about 10 nm) when two different compatibilizer were involved. The marked difference, however, is that the compatibilizer content that resulting in the minimum thickness of the interface shifted to higher level when SMA with less MA content was employed. From the perspective of interfacial layer thickness, there might exist an optimum amount of SMA added.

There are some possible reasons accounting for the change of interfacial thickness mentioned earlier. As FTIR results suggested, when SMA compatibilized PC/AES blends are prepared by means of melt blending, compatibilizer molecules chemically linked to the PC phase as a result of reaction between the MA and terminal hydroxyl groups of the PC. Meanwhile SAN chains or segments of SMA make physical contact with the SAN phase of the AES. Therefore, the effect of PC chains and AES chains
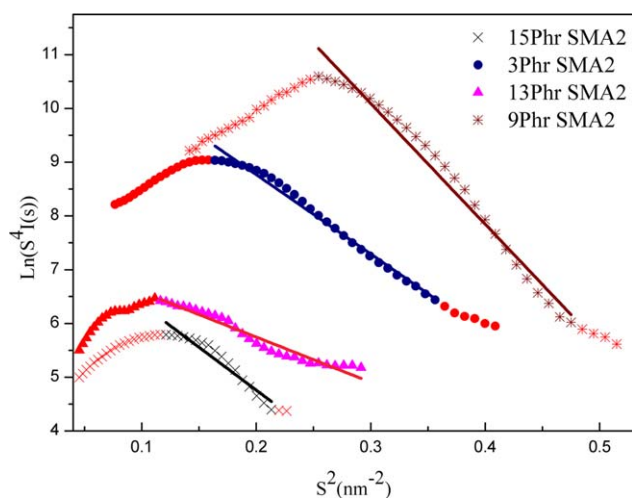
Figure 5. Porod plot in the form of $\ln[I(S)S^4]$ as function of S^2 for SMA2 compatibilized PC/AES (70/30) blends. [Color figure can be viewed in the online issue, which is available at wileyonlinelibrary.com.]

Table II. Interface Layer Thickness of PC/AES (70/30) Blends with and Without SMA as Compatibilizer Determined by SAXS

Polymers	PC/AES (70/30)	3Phr SMA1	9Phr SMA1	11Phr SMA1	3Phr SMA2	9Phr SMA2	13Phr SMA2	15Phr SMA2
E/(nm)	11.8	14.8	10.1	13.6	13.8	16.4	10.0	13.1

spread and twine each other in interface zone is enhanced, which results in a decrease of the interfacial tension between PC phase and disperse phase. Thus, the AES particles can be smaller and dispersed more uniformly in the matrix polymer.

When small amounts of SMA are added to PC/AES blends, the compatibilizing effect mentioned above is not that obvious yet. Although the dispersed domain size decreases slightly, it remains large at this point. And as a result of these larger dispersed domains, SMA that located at the interface zone between PC and AES tend to aggregate into bigger particles. Thus, the space of interface layer is stretched, and thickening of interfacial layer came along with it. After that, with the increase of SMA concentration, the compatibilizing effect becomes more apparent. The smaller the dispersed domain is, the thinner the interfacial layer that surrounding the dispersed domain is. When appropriate amounts of SMA are added to the blends, the interfacial layer thickness detected by SAXS reaches minimum value. Increase as SMA content in blends continuity. Once the concentration of PC-g-MA-co-St copolymer reaches saturation in interface layer, the newly added SMA will diffusion into PC matrix and raises its viscosity by form "micelles."[32–34] These highly grafted micelles aggregates will change the viscosity ratio of PC and AES. Since the component with lower viscosity will encapsulate the more viscous component during processing,[35] the lower-viscosity AES particles trend to coalesce into lager domains. And this is the main factor that contributes to the increase of interfacial thickness at higher compatibilizer level.

Thermal Analysis

DSC thermograms of PC, AES, and PC/AES (70/30) blend are shown in Figure 7. The glass transition temperatures (T_g's) for PC and AES are 147.5 and 109.7°C, respectively (Table III). A clear shift in the T_g of constituent polymers, by blending AES to PC was observed (Figure 7). Such behavior, as already shown elsewhere for PC/SAN blends,[9] is mainly due to the PC/AES blend is partial compatible system. SAN low molecular weight species migrating toward the PC matrix at the interface boundary during the melt-mixing. This increases the AES T_g and plasticizes the PC matrix, lowering its T_g by a classical diluent effect.[36]

Figure 8 shows the DSC curves of PC/AES (70/30) blends compatibilized with various content of SMA1. Resulting data point that came from the analysis of the plot was particularly interesting. A glass transition with an intermediate value between $T_{g(AES)}$ and $T_{g(PC)}$ were observed for some modified blends. It is believe that the T_g can be attributed to the glass transition relaxation of interfacial layer. Comparing with the test results of DSC and SAXS, it becomes obvious that the interfacial layer of these blends has reached considerable size and we can regard it as an independent phase.

When the content of compatibilizer was less than 9 phr, with increasing SMA1 content in blends, the T_g's of constituent polymers ($T_{g(PC)}$, $T_{g(AES)}$) moved closer to each other (Table III) and the intensity of glass transition relaxation peak of interfacial phase was strengthened simultaneously (Figure 8), indicating increased partial miscibility. Moreover, only one T_g was observed in the DSC curve of sample 9Phr SMA1, which implied that the compatibility between AES and the matrix polymer (PC) was tremendous improved. From the DSC test point of view, the compatibilizer concentration in this condition
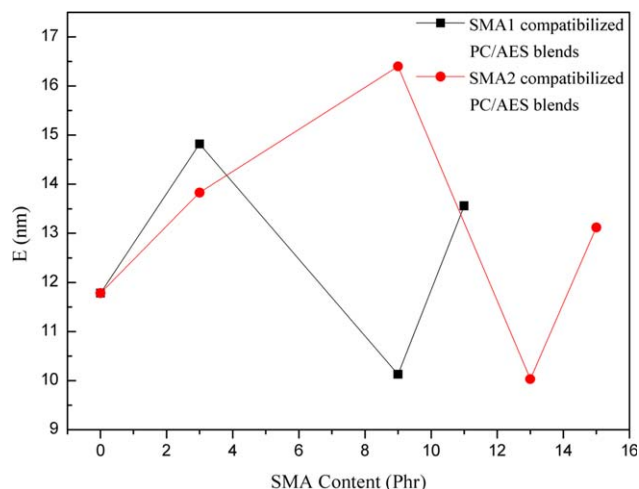
Figure 6. Variation of E with the SMA content in PC/AES (70/30) blends. [Color figure can be viewed in the online issue, which is available at wileyonlinelibrary.com.]
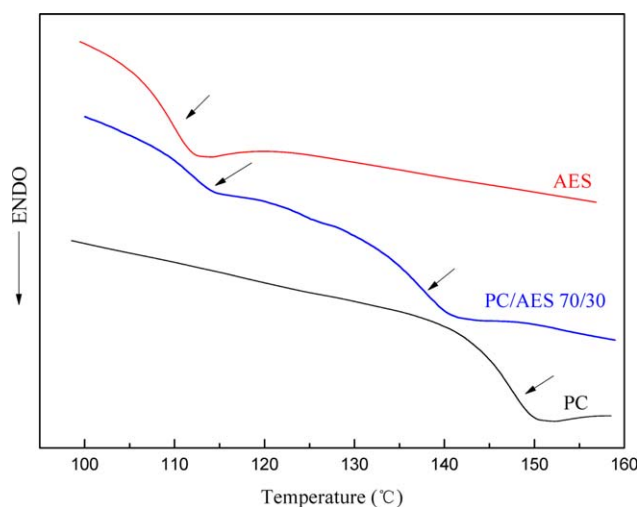
Figure 7. DSC curves of PC, AES, and PC/AES (70/30) blends. [Color figure can be viewed in the online issue, which is available at wileyonlinelibrary.com.]

Table III. Effect of the SMA1 Content on the Glass Transition Parameters of the SMA1 Compatibilized PC/AES (70/30) Blends

Items	Pure PC	Pure AES	PC/AES (70/30)	1Phr SMA1	3Phr SMA1	7Phr SMA1	9Phr SMA1	11Phr SMA1	13Phr SMA1	15Phr SMA1
$T_{g(PC)}$ (°C)	147.5	–	139.7	137.2	136.2	136.2	134.7	134.7	136.1	137.2
$T_{g(Interfacial\ phase)}$ (°C)	–	–	–	122.8	124.5	125.2	–	123.2	–	–
$T_{g(AES)}$ (°C)	–	109.7	111.8	113.7	115.1	115.6	–	–	119.3	118.2
ΔT_{g1} (°C)[a]	–	–	27.9	23.5	21.1	20.6	–	–	16.8	19.0
ΔT_{g2} (°C)[b]	–	–	18.2	14.4	11.7	11.0	–	11.5	–	–

[a] $\Delta T_{g1} = T_{g(PC)} - T_{g(AES)}$.
[b] $\Delta T_{g2} = T_{g(PC)} - T_{g(Interfacial\ phase)}$.
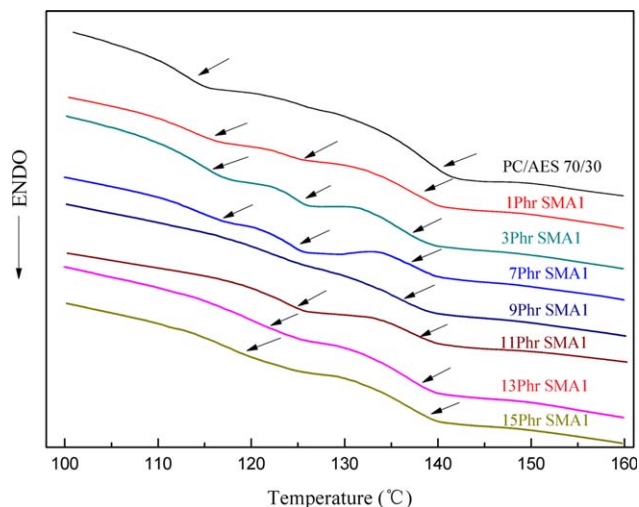
Figure 8. DSC curve of PC/AES (70/30) blends with varying SMA1 reactive components. [Color figure can be viewed in the online issue, which is available at wileyonlinelibrary.com.]

seems to achieve maximum compatibilizing effect for the SMA1 modified PC/AES (70/30) blends. Compatibilizer level beyond this optimum point, two T_g's were detected both in DSC curves of sample 11phr SMA1, 13phr SMA1, and 15phr SMA1. These two T_g's gone away from each other with the level of SMA1 continuing to increase, providing evidence for less partial compatibility.

The DSC thermograms of the PC/AES (70/30) blends comatibilized with different content of SMA2 are exhibited in Figure 9. The corresponding data are listed in Table IV. A clear shift in the glass transition temperature, by changing the content of SMA2 in blends was observed. As SMA2 was added to the blends, $T_{g(AES)}$ monotonically increased and the glass transition temperature for PC of these samples varied in an opposite way. Meanwhile, the T_g with an intermediate value that we can found in SMA1 compatibilized PC/AES blends (Figure 8)
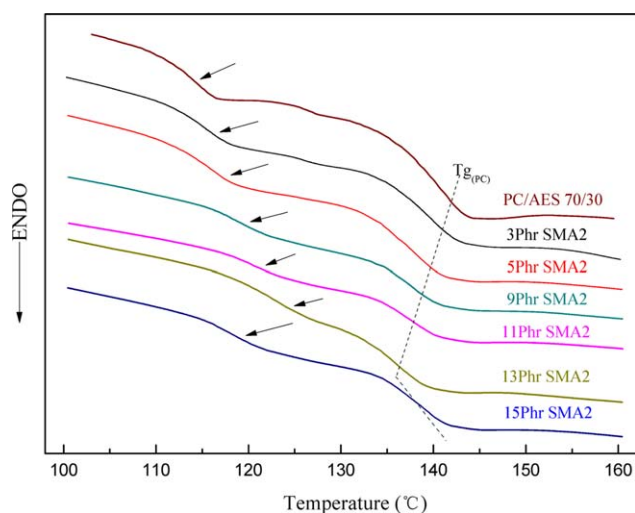
Figure 9. DSC curve of PC/AES (70/30) blends with varying SMA2 reactive components. [Color figure can be viewed in the online issue, which is available at wileyonlinelibrary.com.]

Table IV. Effect of the SMA2 Content on the Glass Transition Parameters of the SMA2 compatibilized PC/AES (70/30) Blends

Items	PC/AES (70/30)	3Phr SMA2	5Phr SMA2	9Phr SMA2	11Phr SMA2	13Phr SMA2	15Phr SMA2
$T_{g(PC)}$ (°C)	139.7	139.5	138.1	137.8	137.9	136.3	139.7
$T_{g(AES)}$ (°C)	111.8	114.8	115.7	118.8	120.4	122.4	117.9
ΔT_g (°C)^a	27.9	24.7	22.4	19	17.5	13.9	21.8

$^a \Delta T_g = T_{g(PC)} - T_{g(AES)}$.

disappeared. After more than 13phr SMA 2 was added to the blends, gaps between two separate glass transition temperatures ($T_{g(PC)}$, $T_{g(AES)}$) increases gradually and provide evidence for less compatibility just like DSC curves of 11Phr SMA1, 13Phr SMA1, and 15Phr SMA1 (Figure 8). Reasons accounting for these phenomena were discussed below.

Morphology Observation
The control of morphology in multiphase blends through reactive compatibilization is an important subject, which has gained increasing attention in recent years.[37,38] The compatibility of incompatible polymer blends can be enhanced by a third com-

ponent that will interact chemically with both phases or will have specific interaction with one phase and physical contact with the other.[39]

Figures 10 and 11 show the SEM photographs of PC/AES (70/30) blends and blends added with different content of SMA as compatibilizer. The strong acids solution leave voids in the PC matrix, which are previously occupied by dispersed AES domains. Because of the poor interfacial interaction between PC and AES, the dispersed particles of PC/AES (70/30) blend without compatibilizer are large in size and elongated in shape, indicating that the morphology of the blend is inferior [Figure
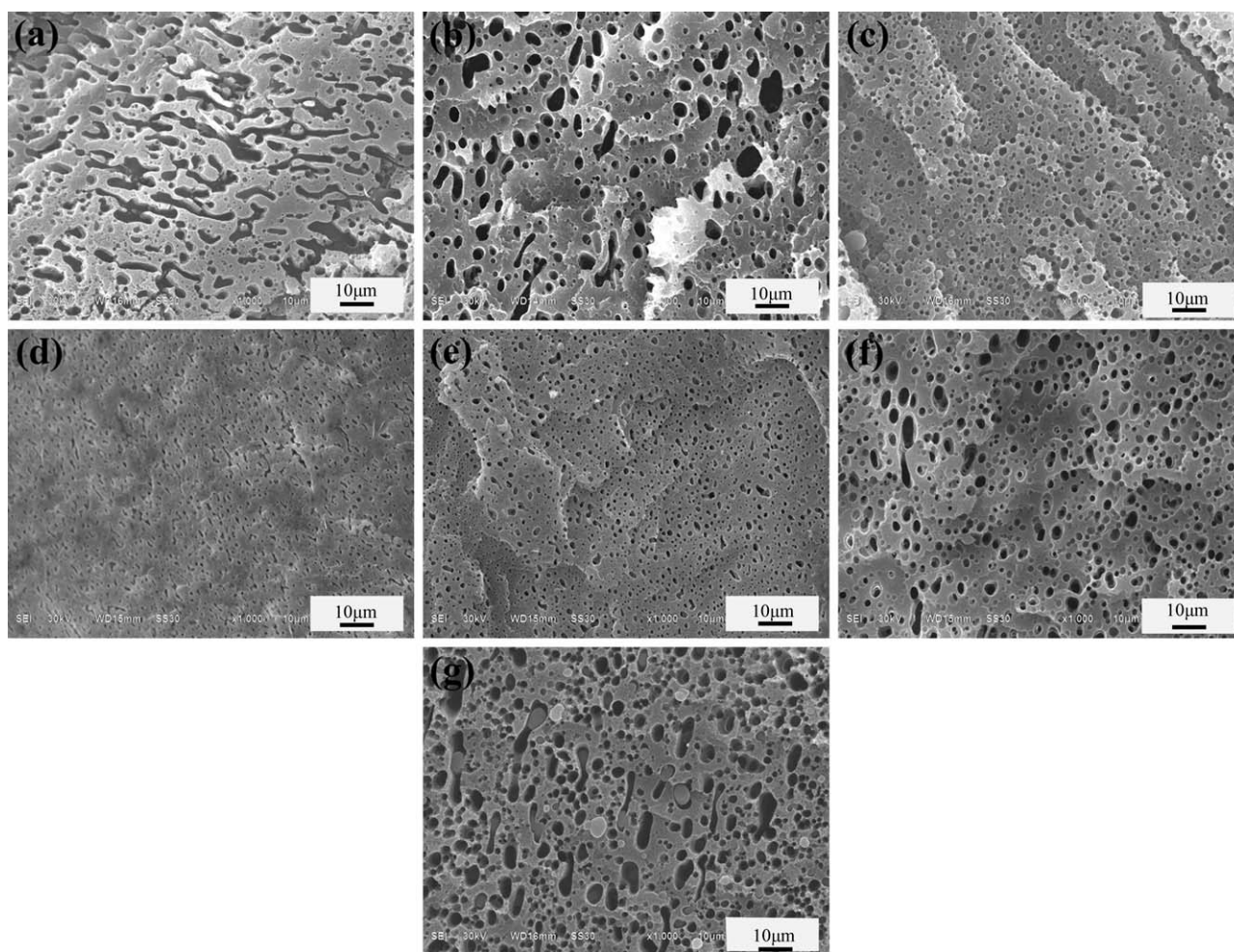
Figure 10. SEM photographs of acid-etched surface of PC/AES (70/30) blends and blends added with SMA1. (a) PC/AES (70/30) blend, (b) 3Phr SMA1, (c) 7Phr SMA1, (d) 9Phr SMA1, (e) 11Phr SMA1, (f) 13Phr SMA1, (g) 15Phr SMA1. All micrographs were taken at the same magnification of ×1000.
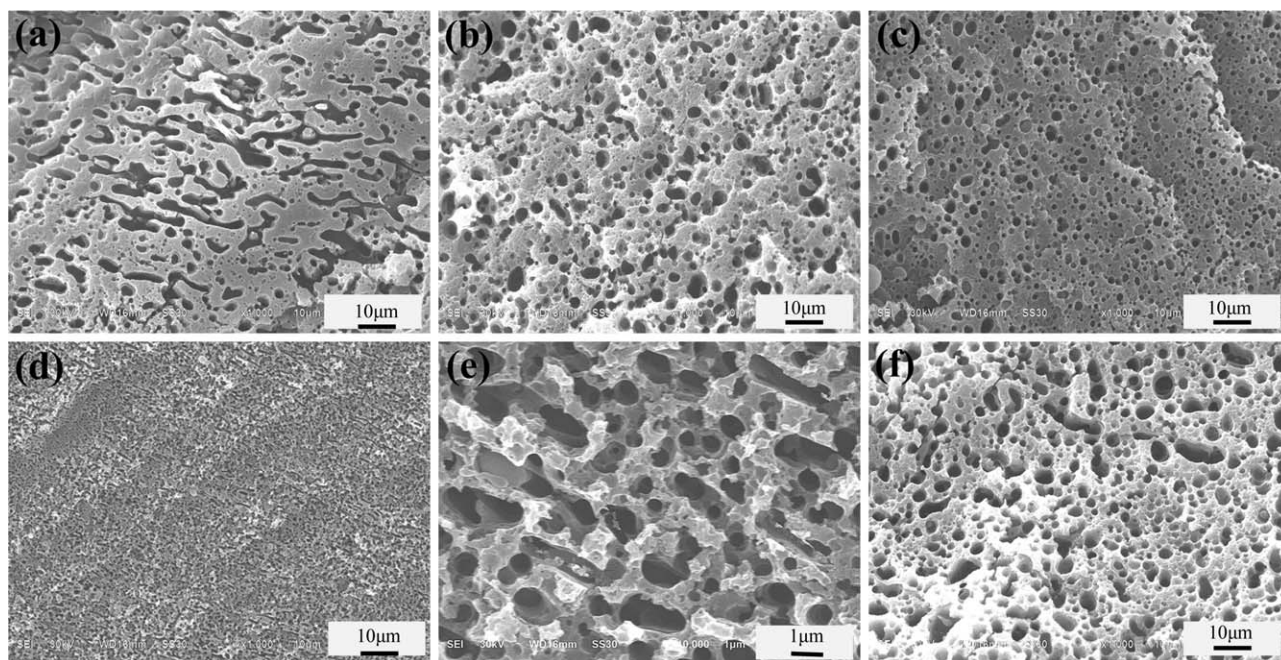
Figure 11. SEM photographs of acid-etched surface of PC/AES (70/30) blends added with SMA2. (a) PC/AES (70/30) blend, (b) 5Phr SMA2, (c) 9Phr SMA2, (d) 13Phr SMA2, (f) 15Phr SMA2. All micrographs were taken at the same magnification of ×1000. (e) 13Phr SMA2 micrograph was taken at the magnification of ×10,000.

10(a)]. With the increase of SMA1 content in blend, the dispersed phase dimension decreases, and even and fine islands-in-sea morphology can be obtained [Figure 10(b–e)].

Figure 10(e) shows the SEM photograph for PC/AES (70/30) blends with 9 phr SMA1. The picture shows that AES particles of the blends form highly dispersed morphology, and the dispersed particles are significantly smaller relative to uncompatibilized blends [Figure 10(a)]. This improvement is attributed to enhancement of interfacial adhesion, which was achieved with the chemical reaction aforementioned.

The morphology of multiphase blends is strongly dependent on viscosity ratio and the magnitude of interfacial tension between the components.[10,40] The component that occupies most space will most likely assume the role of continuous phase. However, the component with lower viscosity will tend to encapsulate the more viscous component, since this reduces the rate of energy dissipation by mixing.[5] But if the viscosity ratio of matrix to dispersed phase and shear rate remain unchanged, then a linear relationship between interfacial tension and the size of dispersion dimension was built.[41] As previously discussed, PC-*g*-MA-*co*-St was generated by the reaction aforementioned. The increase of SMA1 content results in the increase of the concentration of PC-*g*-MA-*co*-St. As an interface compatibilizer, PC-*g*-MA-*co*-St can improve interfacial interaction and decrease interfacial tension. Thus reduce the dispersed particles size. However, levels beyond optimum SMA1 concentration (9Phr SMA1) lead to complex morphology and the dispersed phase no longer remains spherical. Those dispersed droplets become larger, more elongated and distributed unevenly in PC matrix [Figure 10(f–h)]. As stated previously, after the concentration of PC-*g*-MA-*co*-St reaches saturation in interfacial layer, SMA1 will diffusion into PC matrix

and raises viscosity of PC matrix by reaction. Therefore, this effect may lead to enlarge the size of the disperse phase.

Figure 11 shows the effect of SMA2 content on the morphology of PC/AES (70/30) blends. The trend in the change of morphology is quite analogous to blends added with SMA1 (Figure 10). But the optimum ratio of compatibilizer to the blend shifts to higher value as the MA content of the copolymer decreases. SEM observation reveals that the blends added with 13phr of the SMA2 [Figure 11(e)] causes significant reductions in particle size.

Rheological Properties

The linear viscoelastic regions of samples can be easily determined from the response of dynamic modulus to the imposed shear strain. Figure 12 shows the dependence of the storage modulus of the PC, AES, PC/AES (70/30) blend, and SMA compatibilized PC/AES (70/30) blends on the strain at a frequency of 1 rad/s. The results show that the linear viscoelastic region of the AES is far less than that of PC. AES exhibited a linear behavior up to a strain magnitude of 5%, as compared with almost 30% for PC. The linear viscoelastic regions of the PC/AES (70/30) blends and SMA compatibilized PC/AES (70/30) blends are located between those of AES and PC. Therefore, the subsequent measurements were made under a constant strain of 1%.

In melt mixing process, reactions such as grafting, branching or crosslinking may occur. After reaction the overall molecular weight of materials increases, which can lead to an increase in the melt viscosity of the blend system. Therefore, the analysis of the viscosity allows one to indirectly follow the progress of the reactions.[42] Figure 13 shows the dependence of the complex viscosity of PC/SMA blends on frequency. From the figure, it can
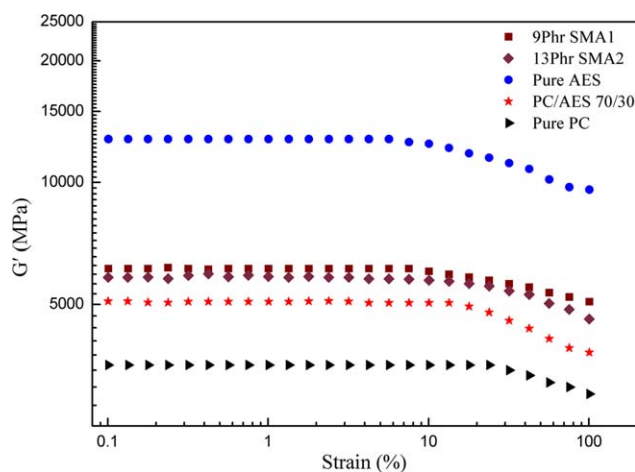
Figure 12. Dynamic modulus versus strain for PC, AES, SMA compatibilized PC/AES (70/30) blends at 250°C and 1 rad/s. [Color figure can be viewed in the online issue, which is available at wileyonlinelibrary.com.]

be seen that the complex viscosity of PC changes slightly with frequency, suggesting that the PC melt is nearly a Newtonian fluid in a broad frequency range. When SMA is blended with PC, the complex viscosities of PC/SMA blends exhibit a more significant shear thinning behavior. The result also shows that the higher SMA content in blends, the higher the viscosity of the blends is. However, small amounts of SMA did not increase the viscosity of the blend. This can be explained in that SMA is a low molecular weight polymer, so the addition of small amount of SMA could decrease the viscosity of the blend by plasticizing effect. But addition large amounts of SMA shows an opposite trend, the complex viscosities of the blends increase a lot. This phenomenon agrees with the claims mentioned before concerning formation of "micelles" in PC matrix.

Mechanism of Interfacial Structural Development
By analyzing the test results of DSC, SAXS, and SEM, it becomes obvious that the interfacial structures of SMA compatibilized PC/AES blends have been of different characteristics as
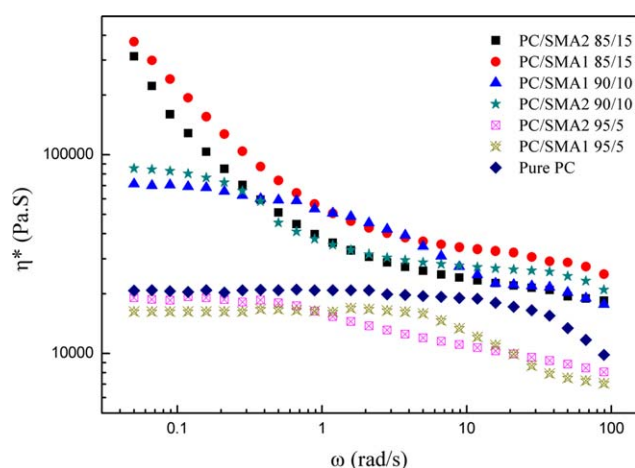
Figure 13. Complex viscosity versus frequency for PC/SMA blends at 250°C. [Color figure can be viewed in the online issue, which is available at wileyonlinelibrary.com.]

the concentration of compatibilizer changes. Hence, mechanism of development of interfacial structural development is proposed for PC/AES (70/30) blends compatibilized with SMA (Figure 14).

Considering that the SAN phase tends to form interface with the PC in the PC/AES blends. Meanwhile, the solubility parameter difference between PC and SAN is small. It will be acceptable to consider that PC chains and SAN chains or segments spread and twine each other on interfacial layer [Figure 14(a)]. Such interfacial structural feature makes glass transition temperatures of constituent polymers move close (Figure 7).

When PC/AES (70/30) blends incorporate with low levels of SMA, the compatibilizer physically contact with the SAN phase of AES and chemically link to the PC phase as a result of reaction between the MA groups of SMA and hydroxyl terminated groups (H) of PC [Figure 14(b)]. Such interfacial structural feature permits more chain entanglement on interface layer than PC/AES (70/30) blends, thus reduces the interfacial tension and improve the compatibility between the dispersed phase and PC matrix. In addition, this interfacial characteristic also leads to strengthen the glass transition relaxation of interfacial phase, and eventually making it detectable by DSC (Figure 8). On the other hand, as SMA locates on the interface layer at a relatively larger size, the space of interface layer is stretched to a certain extent, inherently increasing thickness of interfacial layer (Figure 6). Because of the MA functional group content of SMA1 is higher than SMA2, SMA1 needs more hydroxyl terminated groups to fully react with it. Thus, at the same compatibilizer level, the addition of SMA1 leads to more chain interactions on interface layer than SMA2, and this is the main reason why the three T_g's are only found in SMA1 compatibilized PC/AES (70/30) blends but not in SMA2 compatibilized ones (Figure 9).

As the content of SMA in blends is raised, the effect of the reduction of the dispersed phase size is strengthened due to increase of PC-g-MA-co-St concentration on the interface layer. When appropriate SMA is added to the blends, dispersed domains of the blends are smallest in size and numerous in quantity. Under this circumstance, the dispersed phase has the largest specific surface area, which means the AES phase exhibits the largest contact area with PC matrix. Thereby, SMA particles can disperse uniformly on the interface layer with quite small sizes and less quantity between single dispersed-phase particle and matrix [Figure 14(c)]. Such interfacial structural feature may lead to decrease both the interfacial layer thickness and the intensity of glass transition relaxation of interface-phase. In addition, it should be noted, the concentration of PC-g-MA-co-St may just reaches saturation on interface layer at this point. These unusual interfacial characteristics consistent well with the test results of SAXS and SEM observations since sample 9Phr SMA1 and sample 13Phr SMA2 show minimum thickness of interfacial layer (Table II) and state a minimum dispersion phase size in the respective blending systems.

Because of the concentration of PC-g-MA-co-St reaches saturation at the interface, as the content of SMA continues to increase, SMA will diffuses from interface boundary into PC
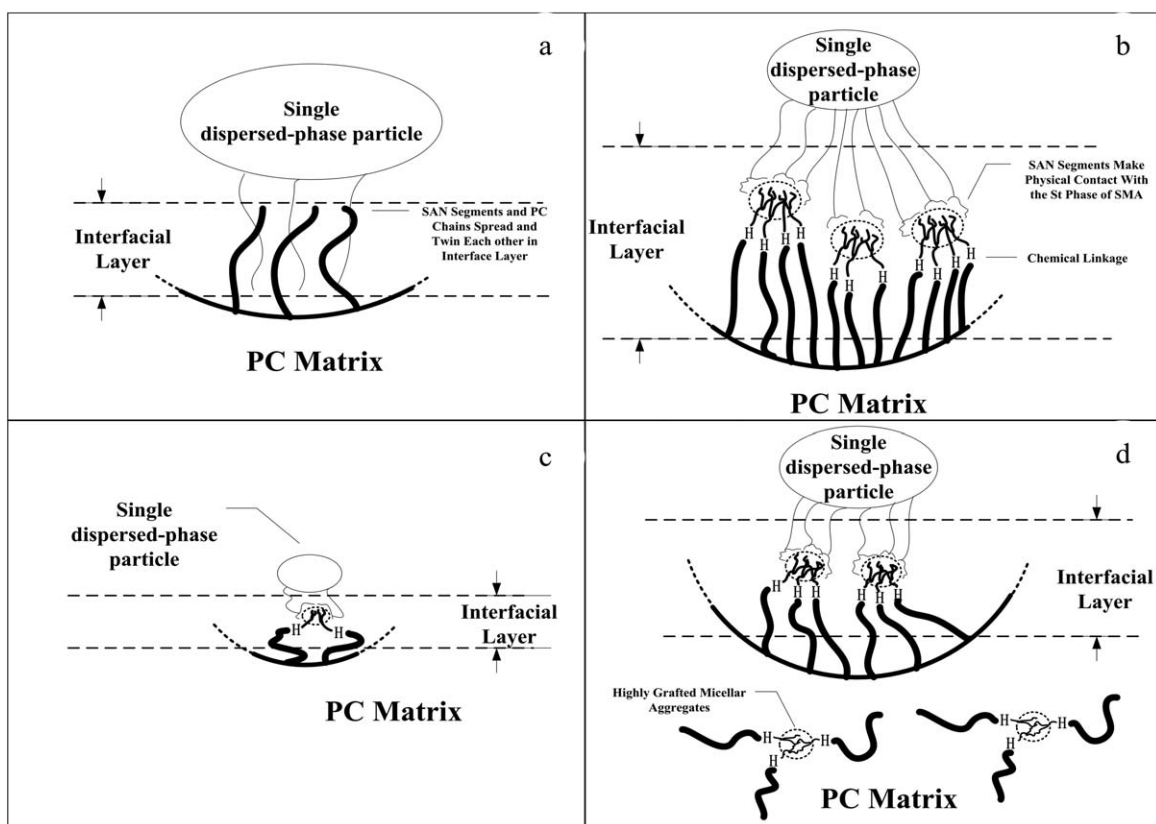
Figure 14. Schematic representations of morphologies and interfacial characteristics of PC/AES (70/30) blends compatibilized by SMA (thin lines represent SAN chains or segments; lines with intermediate thickness represent styrene chains or segments; thick lines represent PC chains).

matrix and form "micelles" [Figure 14(d)]. These highly grafted micellar aggregates will raise PC matrix viscosity by reaction, thereby, the viscosity difference between PC matrix and AES phase is increased, and the lower-viscosity AES trends to coalesce into lager particles. In this instance the dispersed phase has relatively small specific surface area, leading to less reactive sites for anhydride at boundary of the PC phase. Such interfacial characteristics results in less chains interactions in interface

layer, meaning the compatibility between AES and the matrix polymer (PC) is declined. This has been proven by DSC results since $T_{g(AES)}$ and $T_{g(PC)}$ of blends that compatibilized with high SMA content go away from each other (Figures 8 and 9). Furthermore, the interfacial layer thickness of blends added with an excess of SMA is likely to be increased, mainly due to bulk SMA aggregates insert into it. And this interfacial characteristic has been proven by SAXS results (Table II).
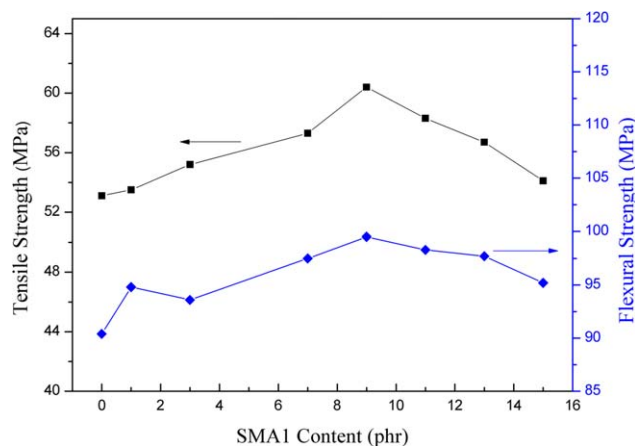
Figure 15. Effect of SMA1 content on tensile and flexural strength of PC/AES (70/30) blends. [Color figure can be viewed in the online issue, which is available at wileyonlinelibrary.com.]
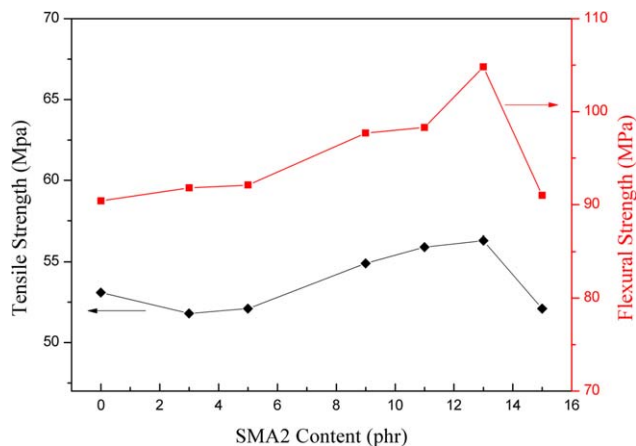
Figure 16. Relationship between tensile and flexural strength of PC/AES (70/30) blends and SMA2 content. [Color figure can be viewed in the online issue, which is available at wileyonlinelibrary.com.]
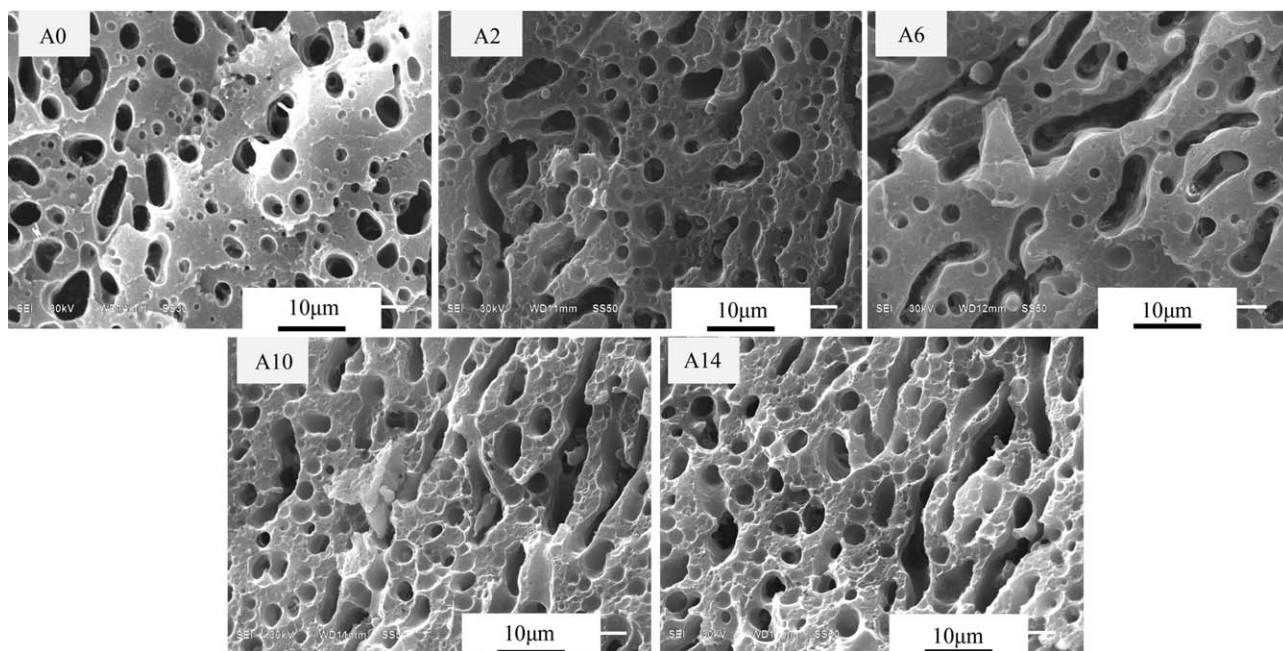
Figure 17. Influence of the annealing time on the phase morphology of PC/AES (70/30) blends at 240°C. (A0) 0 min, (A2) 2 min, (A6) 6 min, (A10) 10 min, and (A14) 14 min. All micrographs were taken at the same magnification of ×2000.

Mechanical Properties

Figures 15 and 16 show the tensile, flexural strength of SMA1 and SMA2 compatibilized PC/AES (70/30) blends as function of compatibilizer content. It is seen from these two figures that tensile strength and flexural strength of PC/AES (70/30) blend are 53.1 and 90.4 MPa, respectively. In both blending systems, with the increasing addition of compatibilizer, tensile strength shows the same change trend as flexural strength.

That is increase at first and decrease afterwards. Therefore, there seems to be an optimum compatibilizer content for well compatibilization effect in this experiment. The best amounts of the compatibilizer content are 9 phr for SMA1 compatibilized PC/AES (70/30) blends and 13 phr for SMA2 compatibilized PC/AES (70/30) blends. These mechanical test results are in good agreement with the previous SEM and DSC test findings.
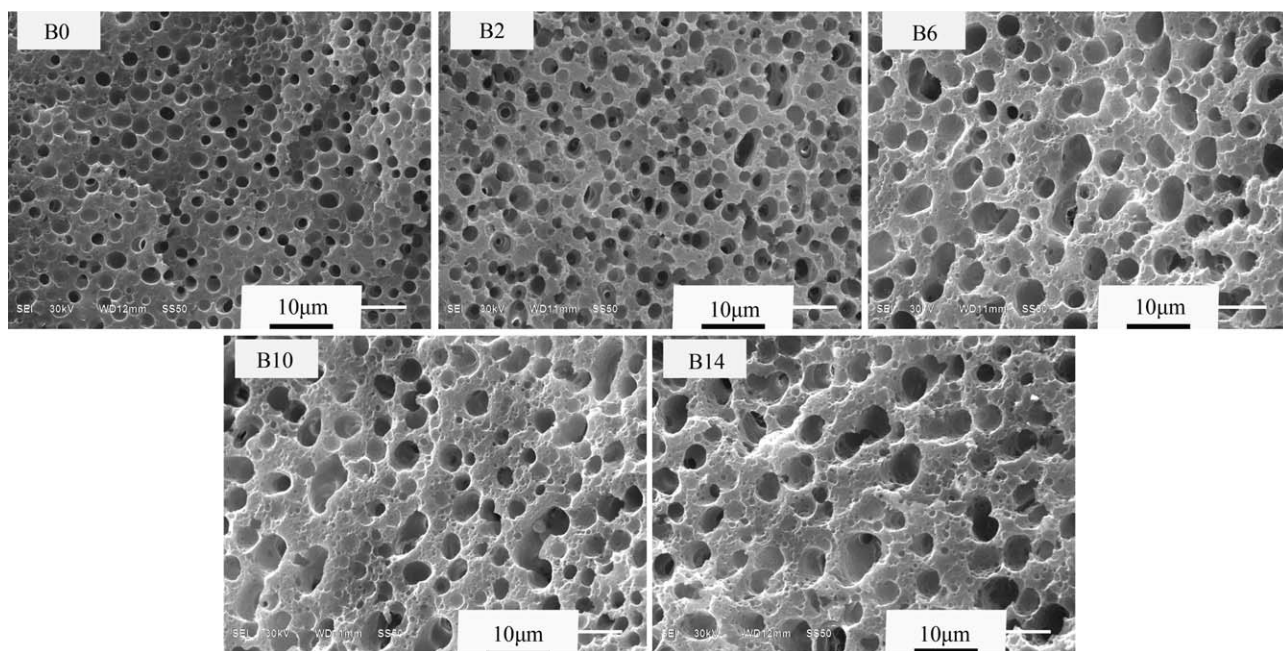
Figure 18. Influence of the annealing time on the phase morphology of 9Phr SMA1 at 240°C. (a) PC/AES (70/30) blend, (B0) 0 min, (B2) 2 min, (B6) 6 min, (B10) 10 min, (B14) 14 min. All micrographs were taken at the same magnification of ×2000.

Effect of Annealing Time on Morphology of Blends

To verify that SMA behaves as a compatibilizer in minimizing dispersed phase coalescence during PC/AES blends processing, injection-molded samples were annealed at 240°C for different time.

Figure 17 shows the result of different annealing time of PC/AES (70/30) blend. From the picture is not difficult to find that when annealing without SMA, the phase morphology will be dramatically altered. Moreover, with the increase of annealing time, obvious coarsening behavior of AES particles is observed. In addition, a tendency of phase transition from a dispersion of AES in a matrix of PC to a co-continuous phase structure is observed. However, when the annealing time exceed 10 min, continuing prolong the annealing time, no significant further coarsening of the PC/AES (70/30) blend was found. Such a dramatic morphological change can leading to the deterioration of the mechanical properties as it can occur in the course of injection or compression molding. The same annealing experiments performed on the injection-molded 9Phr SMA1 also result in phase coarsening as shown in Figure 18. Comparing the dispersed morphology of sample 9Phr SMA1 with PC/AES (70/30) blend, there is a remarkable difference, AES domains of sample 9Phr SMA1 always dispersed unanimously in PC matrix with increasing the annealing time. The trend of forming cocontinuous phase structure has not been realized in sample 9Phr SMA1. Moreover, no significant further coarsening of sample 9Phr SMA1 is evident for annealing times between 6 and 14 min. Hence, such a result confirms that SMA acts as a compatibilizer and as should be minimizes coalescence of the AES domains. This might be due to the *in situ* formed compatibilizer affects the AES domains interface mobility and thereby hinders the AES coalescence and stabilizes the dispersions to the fine morphology during processing.

CONCLUSIONS

The effects of SMA concentration and composition on the behavior of PC/AES (70/30) blends, correlating their interfacial characteristics and phase morphology have been investigated. The major conclusions of the present study are as follows:

i. SMA has good compatibilization for PC/AES (70/30) blend. This is related to the decrease of the interfacial tension between constituent polymers as the PC-g-MA-co-St copolymers produced in the process of the SMA compatibilized PC/AES (70/30) blends. There is a critical concentration for the SMA, when the content is larger than this optimum concentration, the addition of compatibilizing agent have no more positive effect on the interface. This suggests a saturation effect of the in situ grafted copolymers at the interface layer of constituent polymers.

ii. Blends compatibilized by SMA with lower MA content shows two glass transition temperatures. But a extra glass transition with an intermediate value between Tg(AES) and Tg(PC), corresponding to interfacial layer is found in blends compatibilized by SMA with higher MA content. Furthermore, the optimum ratio of compatibilizer to the blend shifts to higher value as the MA content of SMA decrease.

iii. Along with the increasing content of SMA in blends, interfacial thickness is found to: first increase, then decrease to a specific value and increase again. And the compatibilizer concentration that leads to minimum thickness of interface layer is exactly the same as it was when blends exhibited optimal compatibility in DSC tests and SEM observations.

iv. Mechanism of interfacial structural development is proposed for SMA compatibilized PC/AES blends, which predicts the changes in compatibility of PC/AES blends and thickness variation of interfacial layer are due to the changes in the quantity of chains interactions and the dimension variation of SMA located at PC-SAN interface layer.

v. SMA acts as a compatibilizer can improve the tensile and flexural strength of PC/AES (70/30) blend in some degree. Besides, PC/AES (70/30) blend incorporate appropriate amount of SMA has a positive effect on minimizing coalescence of the AES domains during processing.

REFERENCES

1. Wildes, G.; Keskkula, H.; Paul, D. R. *Polymer* **1999**, *40*, 7089.

2. Liu, X.; Bertilsson, H. *J. Appl. Polym. Sci.* **1999**, *74*, 510.

3. Chaudhry, B. I.; Hage, E.; Pessan, L. A. *J. Appl. Polym. Sci.* **1998**, *67*, 1605.

4. Fang, Q. Z.; Wang, T. J.; Li, H. M. *Polymer* **2006**, *47*, 5174.

5. Ishikawa, M. *Polymer* **1995**, *36*, 2203.

6. Greco, R.; Sorrentino, A. *Adv. Polym. Technol.* **1994**, *13*, 249.

7. Greco, R.; Astarita, M. F.; Sorrentino, A.; Dong, L. *Adv. Polym. Technol.* **1994**, *13*, 259.

8. Kim, W. N.; Burns, C. M. *Polym. Eng. Sci.* **1988**, *28*, 1115.

9. Lee, M. P.; Hiltner, A.; Baer, E. *Polymer* **1992**, *33*, 675.

10. Lee, M. P.; Hiltner, A.; Baer, E. *Polymer* **1992**, *33*, 685.

11. Despinasse, M. C.; Schartel, B. *Polym. Degrad. Stab.* **2012**, *97*, 2571.

12. Feyz, E.; Jahani, Y.; Esfandeh, M. *J. Appl. Polym. Sci.* **2011**, *120*, 3435.

13. Peascoe, W. J. US Pat. 4,202,948 (**1980**).

14. Morimoto, M. *J. Appl. Polym. Sci.* **1981**, *26*, 261.

15. Liu, B.; Zhang, Y.; Wan, C.; Shou, W.; Zhang, Y.; Su, Y.; Ji, J. *J. Macromol. Sci.: Phys.* **2006**, *45*, 987.

16. Liu, B.; Zhang, Y.; Wan, C.; Shou, W.; Zhang, Y.; Su, Y.; Ji, J. *J. Macromol. Sci.: Phys.* **2006**, *45*, 1159.

17. Larocca, N. M.; Hage, E.; Pessan, L. A. *Polymer* **2004**, *45*, 5265.

18. Chiantore, O.; Guaita, M.; Lazzari, M.; Ravanetti, G. P. *Polym. Degrad. Stab.* **1995**, *47*, 141.

19. Krause, S. *J. Macromol. Sci.: Polym. Rev.* **1972**, *7*, 251.

20. Quintens, D.; Groeninckx, G.; Guest, M.; Aerts, L. *Polym. Eng. Sci.* **1990**, *30*, 1474.

21. Yang, K.; Lee, S. H.; Oh, J. M. *Polym. Eng. Sci.* **1999**, *39*, 1667.

22. Cheng, T.; Keskkula, H.; Paul, D. R. *J. Appl. Polym. Sci.* **1992**, *45*, 1245.

23. Elmaghor, F.; Zhang, L.; Fan, R.; Li, H. *Polymer* **2004**, *45*, 6719.

24. Balakrishnan, S.; Neelakantan, N. R.; Nabi Saheb, D.; Jog, J. P. *Polymer* **1998**, *39*, 5765.

25. Balakrishnan, S.; Neelakantan, N. R.; Jaisankar, S. N. *J. Appl. Polym. Sci.* **1999**, *74*, 2102.

26. Tjong, S. C.; Meng, Y. Z. *Eur. Polym. J.* **2000**, *36*, 123.

27. Lim, J. C.; Cho, K. Y.; Park, J. K. *J. Appl. Polym. Sci.* **2008**, *108*, 3632.

28. John, J.; Tang, J.; Yang, Z.; Bhattacharya, M. *J. Polym. Sci. Part A: Polym. Chem.* **1997**, *35*, 1139.

29. Scott, C.; Macosko, C. *J. Polym. Sci. B: Polym. Phys.* **1994**, *32*, 205.

30. Koberstein, J. T.; Morra, B.; Stein, R. S. *J. Appl. Crystallogr.* **1980**, *13*, 34.

31. Porod, G. *Kolloid Z.* **1951**, *124*, 83.

32. Wu, S. *Polym. Eng. Sci.* **1987**, *27*, 335.

33. Majumdar, B.; Keskkula, H.; Paul, D. R. *Polymer* **1994**, *35*, 4263.

34. Serpe, G.; Jarrin, J.; Dawans, F. *Polym. Eng. Sci.* **1990**, *30*, 553.

35. Tan, Z. Y.; Xu, X. F.; Sun, S. L.; Zhou, C.; Ao, Y. H.; Zhang, H. X.; Han, Y. *Polym. Eng. Sci.* **2006**, *46*, 1476.

36. Greco, R.; Iavarone, M. *Polym. Eng. Sci.* **2000**, *40*, 1701.

37. White, J. L.; Min, K. *Adv. Polym. Technol.* **1985**, *5*, 225.

38. Xanthos, M. *Polym. Eng. Sci.* **1988**, *28*, 1392.

39. Roder, J.; Oliveira, R. V. B.; Goncalves, M. C.; Soldi, V.; Pires, A. T. N. *Polym. Test.* **2002**, *21*, 815.

40. Mamat, A.; Vu-Khanh, T.; Cigana, P.; Favis, B. D. *J. Polym. Sci. Part B: Polym. Phys.* **1997**, *35*, 2583.

41. Triacca, V. J.; Ziaee, S.; Barlow, J. W.; Keskkula, H.; Paul, D. R. *Polymer* **1991**, *32*, 1401.

42. Arostegui, A.; Na'zabal, J. *J. Polym. Sci. Part B: Polym. Phys.* **2003**, *41*, 2236.